Neutron capture cross section of ^{197}Au: A standard for stellar nucleosynthesis

W. Ratynski* and F. Käppeler
Kernforschungszentrum Karlsruhe, Institut für Kernphysik, D-7500 Karlsruhe, Federal Republic of Germany
(Received 19 October 1987)

We have measured the neutron capture cross section of gold using the ^{7}Li(p,n)^{7}Be reaction for neutron production. This reaction not only provides the integrated neutron flux via the ^{7}Be activity of the target, but also allows for the simulation of a Maxwellian neutron energy spectrum at $kT=25$ keV. As this spectrum is emitted in a forward cone of 120° opening angle, the cross section can be measured in good geometry and independent of any other standard. Systematic uncertainties were studied experimentally in a series of activations. The final stellar cross section at $kT=25$ keV was found to be 648±10 mb, and extrapolation to the common *s*-process temperature $kT=30$ keV yields 582±9 mb. This result is used for renormalization of a number of cross sections which had been measured relative to gold.

I. INTRODUCTION

The importance of the neutron capture cross section of gold as a standard in the keV region initiated a number of measurements. In the energy range of astrophysical interest around 30 keV neutron energy, differential data obtained with time-of-flight (TOF) techniques as well as data obtained with the activation technique are available. Conversion of these results to stellar cross sections is achieved by folding with the Maxwellian neutron energy distribution

$$\Phi \sim E_n \exp(-E_n/kT) \ . \tag{1}$$

For nucleosynthesis by slow neutron captures (*s* process) the common thermal energy is $kT=30$ keV, corresponding to temperatures of 3.5×10^{8} K, as they are typical for helium burning in red giant stars. According to the definition

$$\frac{\langle \sigma v \rangle}{v_T} = \frac{2}{\sqrt{\pi}} \frac{\int_0^\infty \sigma(E_n) E_n \exp(-E_n/kT) dE_n}{\int_0^\infty E_n \exp(-E_n/kT) dE_n} \ , \tag{2}$$

the stellar capture cross section can easily be derived from differential data, $\sigma(E_n)$. Here, E_n is the total kinetic energy in the center-of-mass system. The factor $2/\sqrt{\pi}$ comes from the normalization of the Maxwellian flux formula, using the mean thermal velocity $v_T=(2kT/m)^{1/2}$ (m being the reduced mass) instead of the average velocity. Table I collects all recent gold cross sections, while data prior to 1971 are represented by the evaluation of Allen, Gibbons, and Macklin.[1] The respective experimental cross sections for 30±3 keV are listed in column 4. Maxwellian averages were calculated if the differential data covered a sufficiently large energy range. Otherwise, the 30 keV value was simply multiplied by the factor $2/(1.05\sqrt{\pi})$; this approximation was derived from the data of Macklin[2] and accounts for the fact that the cross section falls slightly steeper than $E_n^{-0.5}$.

Inspection of Table I shows a confusing situation: Most Maxwellian averages[3–6] group around 640±20 mb, except the values of Macklin[2] and of Yamamuro *et al.*,[7] which are at 590±20 mb, but with both groups being characterized by similar uncertainties. In view of this discrepancy and because of their relevance for the present study, the measurements of Macklin[2] and of Zhu *et al.*[6] will be discussed in more detail.

The data given by Macklin[2] were obtained in a measurement of Macklin, Halperin, and Winters,[8] but were later revised at energies below ~100 keV due to an error in data processing. These cross sections were measured relative to the ^{6}Li(n,α) cross section between 3 and 550

TABLE I. Comparison of Maxwellian averaged cross sections for $kT=30$ keV derived from existing experiments.

Reference	Year	Comment	30±3 keV (mb)	$\langle \sigma v \rangle / v_T$ (mb)
Allen, Gibbons, and Macklin (Ref. 1)	1971	evaluation		600±50
Czirr and Stelts (Ref. 3)	1973	differential	585±17	626±19
Gwin *et al.* (Ref. 4)	1976	differential	620±50	663±45
Kononov *et al.* (Ref. 5)	1977	differential	589±30	630±34
Macklin (Ref. 2)	1982	differential	549±14	588±15
Yamamuro *et al.* (Ref. 7)	1983	differential	564±33	599±37
Zhu *et al.* (Ref. 6)	1984	activation	592±18	634±20

keV, and were normalized to an absolute scale via the saturated resonance technique, using the 4.9 eV resonance in gold. However, the quoted uncertainty of 1.4% at 30 keV did not account for possible differences in the capture gamma-ray spectrum between this resonance and the investigated energy range. Therefore, a 2.5% overall uncertainty appears more appropriate. These results were considered as a cross section standard at keV neutron energies in many other experiments.[9]

Neutron production by means of the ^{7}Li(p,n)^{7}Be reaction has the unique feature that the ^{7}Be activity directly represents the time-integrated neutron yield, thus allowing for absolute cross section measurements. If the proton beam energy is kept close to the reaction threshold at $E_p = 1881$ keV all neutrons are kinematically collimated in a forward cone, providing for a "good" experiment geometry. As neutron capture in gold leads to ^{198}Au with a convenient half-life of 2.6 d, the capture cross section can be determined completely by activation.[6,10] From Table I, the activation result[6] appears somewhat higher compared to the differential value.[2] One reason for this discrepancy may be that the neutron spectra during these activations were not determined explicitly; hence the effect of cross section fluctuations could not be corrected for. Another reason for the slightly larger activation values[6,10] may be the use of flat samples adjacent to the neutron target. Even at the reaction threshold, the kinematically collimated neutrons do have emission angles up to $\pm 20°$, and therefore experience a larger effective sample thickness (see Secs. II and IV).

In principle, the activation method allows for cross section measurements at the 1–2 % level, provided that all systematic effects are properly accounted for. In view of the discrepancies among existing data and the need for an accurate standard in forthcoming precise (n,γ) studies with a new 4π BaF_2 detector,[11,12] we considered it worthwhile to reinvestigate the potential of the activation technique. As we were mainly interested in the stellar neutron capture rate, the simulated Maxwell spectrum from the ^{7}Li(p,n)^{7}Be reaction was chosen for the activations. In particular, we intended (i) to exactly characterize the neutron spectrum, and (ii) to study systematic effects experimentally by variation of all critical parameters. The results so obtained should be insensitive to cross section fluctuations because of the broad neutron spectrum.

By means of this absolute cross section for $kT = 25$ keV, the differential data can be renormalized to calculate the stellar capture rate for a wide range of possible thermal energies kT. Furthermore, previous cross sections which are based on the gold standard can then be revised according to the new value.

II. NEUTRON SPECTRUM

Besides the fact that the ^{7}Li(p,n)^{7}Be reaction allows for an absolute cross section determination via the associated ^{7}Be activity, it was also shown to almost perfectly imitate a Maxwellian energy distribution for $kT = 23.4$ keV;[13] this value was later revised to $kT = 25$ keV.[14] As a precise cross section measurement also requires the exact knowledge of the neutron spectrum, the quasistellar spectrum was remeasured with improved sensitivity and over a larger energy range.

Figure 1 shows the experimental setup consisting of two ^{6}Li glass detectors. A stationary monitor 70 cm from the neutron target was used to normalize the spectra obtained at various angles with the second movable detector. The angle-dependent neutron spectra were measured with the TOF technique. The accelerator was

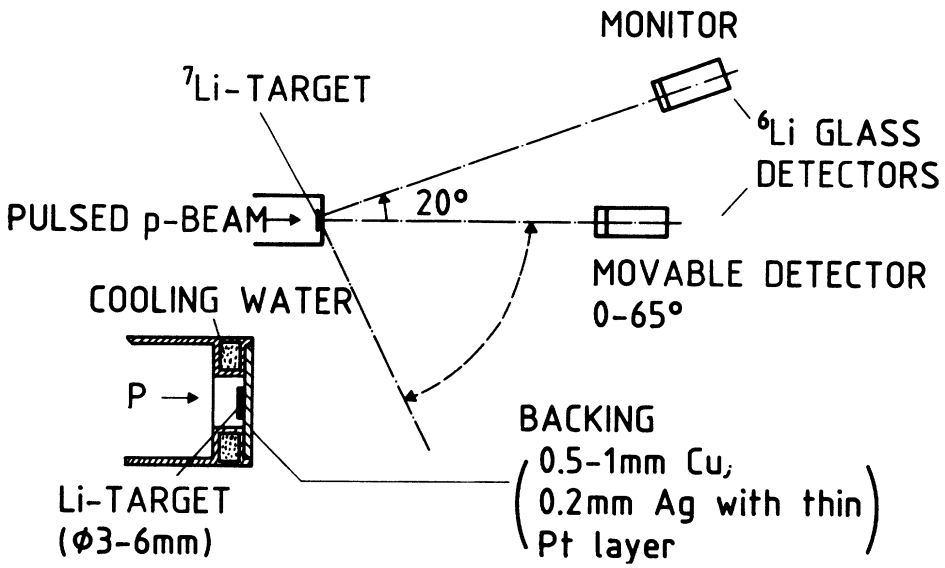

FIG. 1. Experimental setup for determination of the neutron spectrum. The inset shows details of the target construction.

operated in the pulsed mode at a repetition rate of 1 MHz and a pulse width of ~ 1 ns. The proton energy $E_p = 1912$ keV was chosen as in the previous study,[13] leading to a kinematic neutron collimation into a cone of 120° opening angle. In addition, a second spectrum with $E_p = 1914$ keV was also measured in order to study the effect of an eventual uncertainty in proton beam energy. It should be emphasized, however, that this 2 keV difference is much larger than the stability limits of standard Van de Graaff accelerators. This is the more true for the Karlsruhe machine, which is under continuous computer supervision during operation.

The spectrum measurements were carried out in two steps: The energy range $5 < E_n < 120$ keV was measured with the movable detector located at a flight path of 51.5 cm. Then, the flight path was reduced to 27.8 cm in order to improve the sensitivity at low energies. In this way the measurements could be extended down to ~ 1 keV. The TOF spectra were measured in steps of 5° between 0° and 65°, normalized to the monitor spectrum and finally corrected for solid angle and for the efficiency of the ^{6}Li glass detector. The most significant contributions come from the angular range between 20° and 30°, while practically no neutrons are observed at 65°. Figure 2 shows these spectra on a neutron energy scale; statistical uncertainties are negligible in these measurements.

Integration over the entire neutron cone yields the final spectra given by histograms in Fig. 3. For the standard proton energy of 1912 keV (top) the neutron spectrum ends at $E_n^{max} = 106$ keV and includes the results obtained at the short flight path (open squares). For comparison, the complementary measurement at 1914 keV proton energy yielded an almost identical spectrum (bottom). The maximum neutron energy is 114 keV and the opening angle of the neutron cone 132°. The solid lines represent least squares fits of Maxwellian distributions, which show good agreement for the two spectra. In particular, the fit is almost perfect from 80 keV down to the lowest neutron energies. This is an important result because the cross sections scale with E_n^{-x}, the power x ranging typically from 0.5 to 0.8; therefore, the low energy region contributes strongly to the stellar rate [Eq. (2)]. This means also that the difference between the actual spectra and the true Maxwellian shape at higher energies does not have a significant impact on the final cross section. This point can be illustrated explicitly by folding the differential gold cross section[2] with the experimental spectrum and with the Maxwell distribution (Sec. IV). The important result of these measurements is that (i) the ^{7}Li(p,n)^{7}Be reaction can be used to imitate a thermal stellar neutron spectrum, (ii) the thermal energy of this spectrum is not very sensitive to proton energy, and (iii) for a proton energy of 1912 keV (corresponding to a maximum neutron energy of 106 keV) the thermal energy is $kT = 25.0 \pm 0.5$ keV.

As has been mentioned by Käppeler *et al.*,[15] a Maxwell spectrum can be approximated up to higher neutron energies simply by further raising the proton energy; but then the forward collimation of the neutron beam is lost, and the 120° neutron cone must be defined via the solid angle between neutron target and sample.

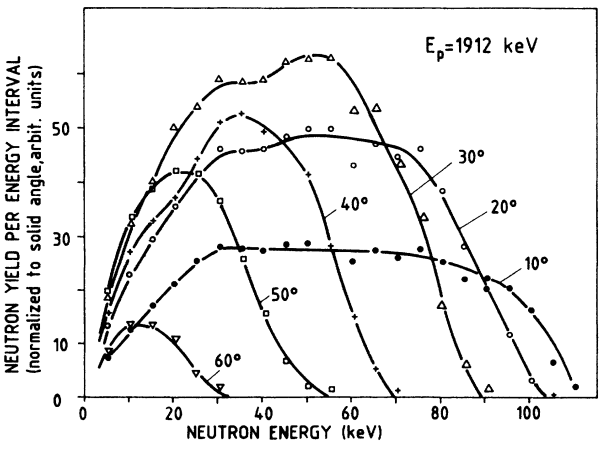

FIG. 2. Neutron spectra obtained from the ^{7}Li(p,n)^{7}Be reaction at different emission angles.

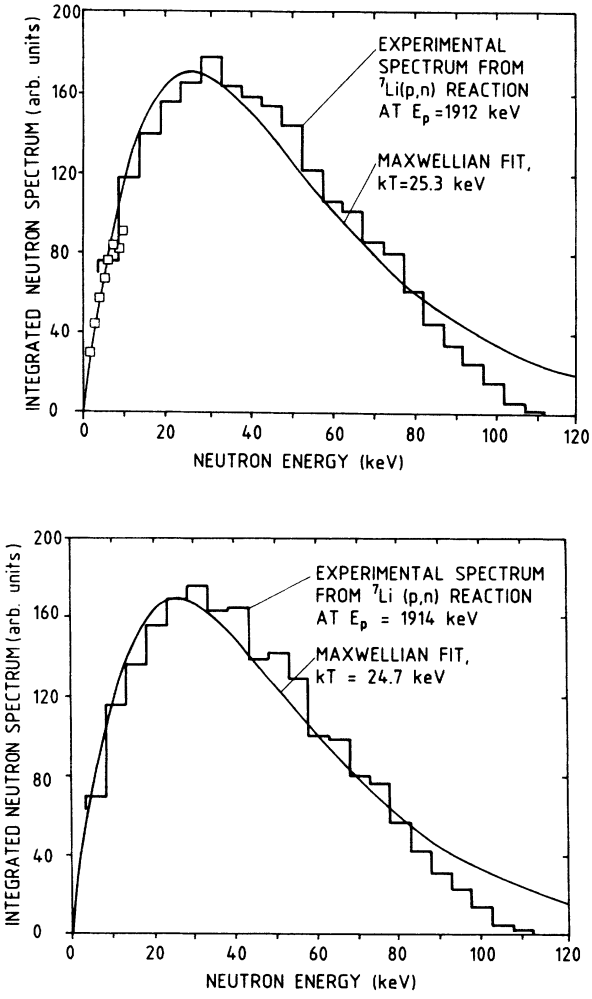

FIG. 3. Total neutron spectrum after integration over all emission angles, for proton energies $E_p = 1912$ keV (top) and 1914 keV (bottom). The squares are the result of the measurement at short flight path.

Aside from the crucial drawback for the present technique that the ^{7}Be activity would no longer correspond to the total neutron exposure of the sample, corrections due to neutron scattering in the target area would become a severe problem.

Previous activation measurements often assumed a neutron spectrum around 30 keV from the ^{7}Li(p,n)^{7}Be reaction near threshold without an explicit experimental verification. Therefore, we also investigated the spectrum that is obtained directly at the reaction threshold. The proton energy was adjusted such that neutron production was almost zero, and then the beam energy was raised by 2 keV. Given a 1 keV energy spread of the proton beam, this should correspond to $E_p \sim 1882$ keV. The resulting spectrum as plotted in Fig. 4 covers a rather broad range in energy and in angle as well. This latter point may be relevant with respect to the use of flat samples in previous activations measurements.[6,10]

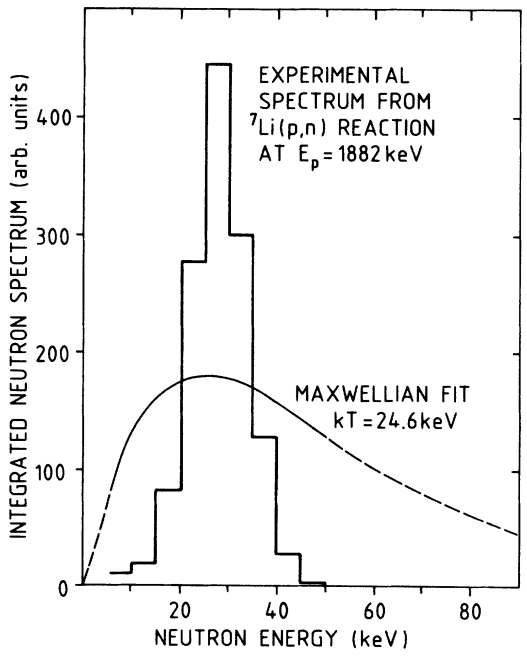

FIG. 4. Neutron yields obtained from the ^{7}Li(p,n)^{7}Be reaction at $E_p = 1882$ keV, 1 keV above the reaction threshold.

III. ACTIVATIONS

The activation measurements were carried out in three steps: Definition of the Au samples, irradiation in the well defined neutron spectrum, and determination of the induced ^{7}Be and ^{198}Au activities.

A. Samples

In the present study, the shape of the Au samples is completely dictated by the experimental technique. The implied conditions are that *all* neutrons pass through the sample and that the sample appears *equally thick* to all neutrons. Consequently, the sample had to be a homogeneous spherical segment covering the entire neutron beam. To ensure complete coverage of the primary neutron beam the sample was chosen to cover a cone of 140° opening angle around the proton beam axis (see Fig. 5). As this holds exactly only for a pointlike neutron source, different ^{7}Li targets of 3, 4, and 6 mm diameter were used in different activations without causing any noticeable effect in the respective results. Great care was spent in producing thin and well-defined samples. These were made from 0.02 and 0.05 mm thick gold foils by deep drawing into a precisely machined tool, the two halves corresponding exactly to the respective foil thickness. In this way, folds produced during deep drawing were completely compensated when the samples were exposed to pressures of some 10^{6} N cm^{-2} for several hours. Then, the samples were carefully cut in a special tool to ensure the exact shape of a spherical segment. With these precautions, the sample thickness N (in atoms per mb) could be determined to a precision of 0.6%. This uncertainty is related to the surface of the sample (as de-

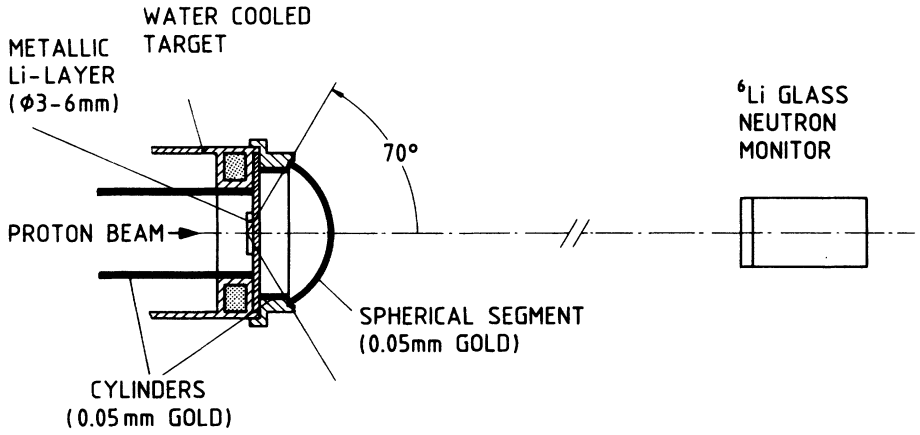

FIG. 5. Experimental setup during the activations. In addition to the spherical gold sample, two gold cylinders were used to detect the effect of scattered neutrons. The sample upstream of the neutron target acts also as a catcher for ^{7}Be sputtered from the target.

rived from the height of the spherical segment of 9.60±0.05 mm, resulting in a 0.6% surface uncertainty), while the mass can easily be obtained to ±0.05 mg (±0.02%). The homogeneity of the samples was checked by transmission of a collimated gamma-ray beam through a regular pattern of 5–9 points on the spherical segment. With the 60 keV gamma rays from an ^{241}Am source, the transmission is 65% for 0.05 mm Au, just the proper range to make this method sensitive. None of the samples showed inhomogeneities in excess of 3%, and—even more important—there was no evidence for systematic differences between the center and the edge. The relevant sample characteristics are included in Table III.

B. Irradiations

All irradiations were carried out at the standard proton energy $E_p = 1912$ keV. This energy was routinely determined by a neutron TOF measurement prior to each activation with the accelerator operated in pulsed mode. The proton energy was adjusted as to obtain the maximum neutron energy of 106±2 keV, a method which is more sensitive and accurate than relying on an accelerator calibration. The accelerator was then switched back to dc mode for the irradiations.

In a number of tests it was found that ^{7}Be losses were negligible, provided the thermal load of the target was not too high. As this holds for metallic Li targets and for LiF as well, all activations were performed with metallic targets because of the higher neutron yield. The thickness of the Li layer was chosen to correspond to a proton energy loss of 100 keV so that all protons are slowed down below the reaction threshold at 1881 keV before being stopped in the target backing. For our target construction cooling was achieved by lateral heat conduction through the backing material itself, an arrangement which is chosen to minimize the problem of neutron scattering. With 1 mm thick Cu backings this target can stand proton currents up to 200 μA without showing significant ^{7}Be losses if the beam is wobbled over an area of 6×6 mm^2. In order to avoid this problem completely, the activations were carried out with beam current densities of less than 1 μA/mm^2, far below the design value. Consequently, the target cooling was sufficient to allow for a significant variation of the backing thickness in order to study experimentally the effect of neutron scattering. The more neutrons are scattered in the target backing the more are lost from the primary beam, resulting in an apparent reduction in Au activity and hence in cross section. Therefore, in addition to the ordinary targets with 1 mm thick backings, 0.5 and 0.7 mm Cu and 0.2 mm Ag backings were also used. (The latter backing was coated by a thin Pt layer to prevent Li from diffusing into the silver.)

Together with the spherical Au sample two cylindrical Au samples were used during the activations as sketched in Fig. 5. These are intended to cover practically all of the remaining solid angle, thus directly detecting scattered neutrons. The activities of these cylinders were found to correlate with backing thickness, and hence allow for an appropriate correction in the evaluation of the true cross section. These corrections are small (1.8% for 1 mm Cu and 0.5% for 0.2 mm Ag) and are considered by the factor K_s in Eq. (3). The cylinder upstream of the neutron target contributed about 40% to this correction, and served also to check for Be losses. Even tiny fractions of the total ^{7}Be activity could be detected in the measurement of the gamma-ray activity. These losses never exceeded 0.2%.

The irradiation times of 1–4 h were chosen to correspond to an integrated beam current on target of about 0.05 Cb. This was sufficient to achieve good statistics in the activity measurement. As the irradiation times were always much shorter than the half-lives of ^{198}Au (2.62 d) and ^{7}Be (53 d), only a small fraction of activated nuclei decayed during irradiation. Nevertheless, the neutron yield was recorded as a function of time throughout all activations for proper determination of this correction.

Neutrons scattered from the walls of the experimental area did not contribute to the activation of the gold samples. This was verified by additional gold foils placed in the plane of the target backing, but outside the normal samples. The activation of these samples was barely detectable, and this background could therefore be completely neglected.

C. Activity measurement

The sample activities were determined via the 412 and 478 keV gamma-ray lines emitted in the decay of ^{198}Au and ^{7}Be, respectively. The relative intensities, I_γ, for these decay modes were adopted from literature to 95.5±0.1 % for gold[16] and to 10.45±0.04 % for beryllium.[17] The half-lives of both isotopes were taken from Lederer and Shirley.[16] The uncertainty introduced by these parameters was negligible as the activity measurement was always shorter than the 2.62 d half-life of gold.

The gamma-ray spectra were taken with a coaxial, high purity Ge detector which had a peak to Compton ratio of 32 and an energy resolution of 1.7 keV at 1.33 MeV. The efficiency of this detector was carefully calibrated in the range $150 < E_\gamma < 800$ keV, using a set of standard sources (Bureau National de Metrologie, Office des Rayonnements Ionisants, F-91190 Gif-sur-Yvette, France) which all were defined to ±1.5% or ±2%. Of course, the mechanical setup was designed to guarantee an exactly reproducible geometry for the calibration as well as in the later activity measurements. The resulting efficiency is plotted in Fig. 6 versus gamma-ray energy. The correlation coefficient $r = 0.9995$ shows that (on the log-log scale) the measured points are perfectly fitted by a straight line. The slope of this line, $b = -1.300\pm0.020$, was therefore used to define the efficiency ratio at the energies of the two gamma-ray lines of interest, 412 and 478 keV. This could be derived with an uncertainty of 0.3%, which simply reflects the uncertainty in extrapolating from 412 keV to the closely neighbored point at 478 keV.

The samples were positioned 76 mm from the Ge detector. It was verified by many repeated runs that this distance was reproducible with negligible effect on the efficiency. However, a correction for extended sources had to be applied for the gold samples, because the

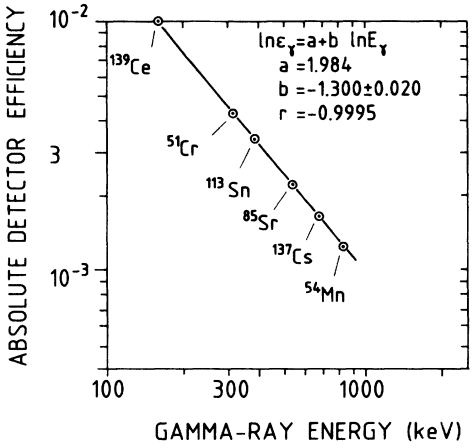

FIG. 6. The efficiency of the HP-Ge detector (HP denotes high purity) used for activity counting. The indicated points were measured with calibrated sources, the line is a least squares fit in the log-log plot.

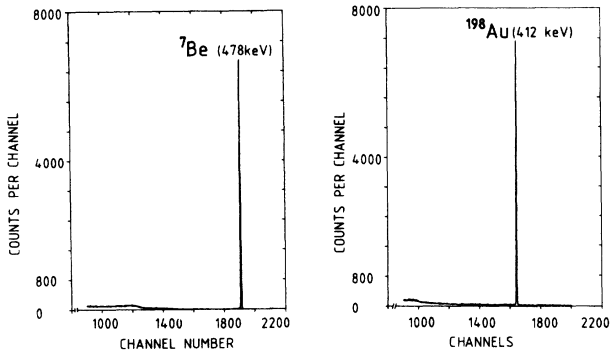

FIG. 7. Gamma-ray spectra from the activity counting of gold (4 h) and beryllium (0.2 h).

spherical segments were pressed to flat irregular disks after irradiation with neutrons. This correction was determined experimentally to $K_\Omega = 0.981 \pm 0.006$ by moving a point source across that surface and by cutting the samples in 3.5 mm broad rings for consideration of the activity distribution. Gamma-ray self-absorption for the gold samples was calculated to $K_\gamma = 0.990 \pm 0.003$. For the ^{7}Be line the transmission through the target backings had to be considered in addition. These corrections were determined experimentally to range between 0.980 and 0.930 (±0.5%). Figure 7 shows the gamma-ray spectra accumulated in 4 and 0.2 h for the gold and the beryllium sample, respectively. The high counting statistics and the low background ensure an accurate intensity determination. Typical counting times were 16–24 h for Au and 1–2 h for Be. Dead time corrections were always negligible. The room background was considerably reduced by a shield of Al, Cu, Cd, and Pb layers and did not show any contaminating lines around 412 and 478 keV.

D. Data analysis

The number of reactions during the irradiations,

$$A = \frac{C/t_m}{\epsilon_\gamma K_\Omega I_\gamma K_\gamma} f_b f_w f_m \frac{1}{K_s} \frac{1}{\lambda} , \tag{3}$$

can be determined from the measured count rate in the ^{198}Au and ^{7}Be lines, C/t_m, corrected for the detector efficiency, ϵ_γ, for the relative gamma-ray intensity per decay, I_γ, and for gamma-ray absorption, K_γ. The factors f_b, $f_w = \exp(-\lambda t_w)$, and $f_m = [1 - \exp(-\lambda t_m)]$ account for the decay during activation, during the waiting time between activation and measurement, and during the measurement itself, and are discussed elsewhere.[13] The last two terms in Eq. (3) denote the correction for neutron scattering in the target, K_s, and the decay rate $\lambda = \ln 2 / t_{1/2}$. The factor K_Ω corrects for the solid angle of extended sources and applies only for the activity

TABLE II. Systematic and statistical uncertainties.

Source of uncertainty		Related uncertainty (%)
Thickness of gold sample, N_γ		0.6
Counting statistics, C_i	Au:	0.4
	Be:	0.3
Ratio of gamma-ray efficiency, ϵ_γ(Be)/ϵ_γ(Au)		0.3
Solid angle for extended sources, K_Ω		0.6
Gamma-ray intensity per decay, I_γ	Au:	0.1
	Be:	0.4
Gamma-ray self-absorption, K_γ	Au:	0.3
	Be:	0.5
Neutron scattering in target, K_s		0.1–0.4
Decay rates, λ	Au:	0.1
	Be:	<0.1
Irradiation history, time factors, f_i		negligible
		Total uncertainty: 1.3–1.4

measurement of the gold samples.

The number of neutron captures in the Au sample can be expressed by the cross section, σ, and the neutron flux, $\Phi(t)$, as

$$A_{\mathrm{Au}}=N\sigma\int\Phi(t)dt\ , \tag{4}$$

with N denoting the sample thickness. The neutron exposure $\int\Phi(t)dt$ follows immediately from the number of beryllium nuclei, A_{Be}. The capture cross section of gold is then obtained from Eqs. (3) and (4):

$$\sigma=\frac{1}{N_{\mathrm{Au}}}\frac{C_{\mathrm{Au}}}{C_{\mathrm{Be}}}\frac{(\epsilon_\gamma I_\gamma K_\gamma)_{\mathrm{Be}}}{(\epsilon_\gamma K_\Omega I_\gamma K_\gamma)_{\mathrm{Au}}}\frac{(f_b f_w f_m)_{\mathrm{Au}}}{(f_b f_w f_m)_{\mathrm{Be}}}\frac{\lambda_{\mathrm{Be}}}{\lambda_{\mathrm{Au}}}\frac{1}{K_s}\ . \tag{5}$$

The uncertainties of the various quantities in Eq. (5) have been discussed above and are summarized in Table II.

IV. RESULTS AND DISCUSSION

The results obtained in eight activations are summarized in Table III. Information on neutron targets and gold samples is included to illustrate the systematic variation of relevant experimental parameters. The individual results exhibit uncertainties between 1.4% and 1.6%, in agreement with the compilation of Table II. The observed scatter of the results being fully consistent with the discussed uncertainties supports the reliability of the experiment. As systematic effects clearly dominate the overall uncertainty, combination of the individual results does not allow for a significantly smaller uncertainty in the final cross section. For the quasistellar neutron spectrum of Fig. 3, which corresponds to a thermal energy of $kT=25.0\pm0.5$ keV, we therefore quote the neutron capture cross section of gold to be $\sigma=586\pm8$ mb.

This experimental result must be slightly modified before it can be used in an astrophysical context. Conversion to a true stellar cross section requires multiplication with the normalization factor $2/\sqrt{\pi}$ of Eq. (2) and a correction for the difference of the experimental neutron spectrum (Fig. 3) from the true Maxwellian shape. The latter correction can be obtained via the differential gold cross section of Macklin.[2] Folding this cross section with a Maxwell spectrum from $E_{\mathrm{n}}=3$ keV to infinity yields an average of $\langle\sigma\rangle_1=557$ mb. If this procedure is repeated with the Maxwell spectrum being truncated at $E_{\mathrm{n}}=110$ keV, one obtains $\langle\sigma\rangle_2=571$ mb, and with the experimental spectrum of Fig. 3 one finds $\langle\sigma\rangle_3=568$ mb. The good agreement between $\langle\sigma\rangle_2$ and $\langle\sigma\rangle_3$ reflects the perfect representation of the experimental distribution below 100 keV by the Maxwell spectrum, while the difference to $\langle\sigma\rangle_1$ corresponds to the contribution from higher energies. This can now be used to convert our experimental cross section to a Maxwellian average according to Eq. (2):

$$\frac{\langle\sigma v\rangle}{v_T}=\frac{2}{\sqrt{\pi}}\frac{\langle\sigma\rangle_1}{\langle\sigma\rangle_3}\sigma_{\mathrm{exp}}=648\ \mathrm{mb}\pm1.5\%\ . \tag{6}$$

TABLE III. Results and relevant parameters for the activations with spherical gold samples.

	Lithium target		Spherical gold segment			Integrated gamma-ray line		Cross	Relative
Activation	Backing (mm)	Diameter (mm)	Mass (mg)	Surface (cm^2)	Thickness (10^{-7} atoms/b)	Au (412 keV) (net counts)	Be (478 keV) (net counts)	section (mb)	uncertainty (%)
1	1.0 (Cu)	6	329.30±.05	8.162±.074	1233±11	158 580±400	235 060±490	589±9	1.6
2	0.5 (Cu)	4	952.45±.05	9.142±.055	3185±19	109 410±330	104 000±325	598±8	1.4
3	1.0 (Cu)	4	1024.30±.05	9.095±.055	3443±21	68 435±265	102 210±320	574±8	1.4
4	0.7 (Cu)	4	987.70±.05	9.113±.055	3313±20	67 910±265	103 170±325	590±8	1.4
5	0.2 (Ag/Pt)	4	977.30±.05	9.095±.055	3286±20	43 790±210	59 370±245	587±9	1.5
6	0.2 (Ag/Pt)	4	987.00±.05	9.142±.055	3301±20	77 630±280	85 340±300	582±8	1.4
7	0.2 (Ag/Pt)	3	1017.95±.05	9.095±.055	3421±21	65 290±260	95 070±310	576±8	1.4
8	0.2 (Ag/Pt)	6	1012.15±.05	9.095±.055	3403±21	54 360±240	57 150±245	595±9	1.5
						Average experimental cross section		586±8	1.4

TABLE IV. Maxwellian averaged gold cross section (renormalized values of Macklin, 1982).

Thermal energy (keV)	$\langle \sigma v \rangle / v_T$ (mb)
10	1206±18
15	904±13
20	746±11
25	648±10
30	582±9
35	533±8
40	496±7
45	467±7
50	444±7
52	426±6

The uncertainty of this conversion was assumed to be characterized by the difference between $\langle \sigma \rangle_1$ and $\langle \sigma \rangle_3$, leading to an overall uncertainty of 1.5%.

By comparison with Macklin's Maxwellian averaged cross section for $kT = 25$ keV, we finally obtain a renormalization factor for the differential cross section

$$R_{\text{norm}} = \frac{648 \pm 10 \text{ mb}}{655 \text{ mb}} = 0.989 \pm 1.5\% \ . \quad (7)$$

This excellent agreement confirms the previous gold cross section of Macklin.[2] At the same time the accuracy of this important standard is improved to ±1.5%. The revised Maxwellian averaged cross sections are listed in Table IV. The comparison with previous results (Fig. 8) shows good agreement with Macklin[2] and Yamamuro *et al.*,[7] while the other values are slightly higher.

It was mentioned in Sec. I that the use of flat samples could be responsible for the somewhat larger cross sections obtained in earlier activation measurements.[6,10] This was checked by an activation where a flat and a spherical gold sample was irradiated simultaneously.

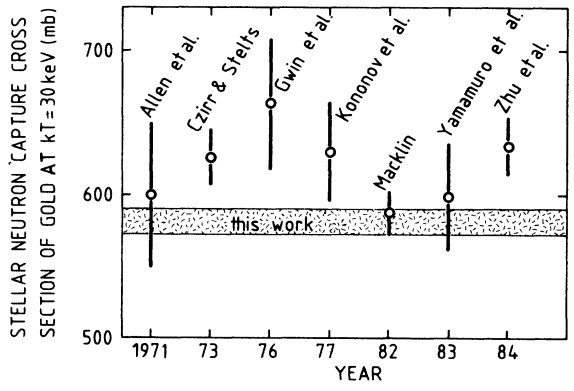

FIG. 8. Comparison between previous measurements and the present result.

Indeed, the so-obtained cross section ratio $\sigma_{\text{sphr}}/\sigma_{\text{flat}} = 0.951$ suggests this effect to cause the observed discrepancy.

V. ASTROPHYSICAL CONSEQUENCES

The present result is in good agreement with the most often used standard values for the capture cross section of gold. The differences to the data of Macklin[2] and to the previously recommended value at $kT = 30$ keV by Bao and Käppeler[9] are 1.1% and 3.5%, respectively, and are not significant for the overall picture of *s*-process nucleosynthesis at the present stage. This may not hold for particular details, but, in general, other uncertainties still dominate in most cases. The importance of the precision achieved in the present study lies in future applications, when improved experimental techniques are expected to yield cross sections at the 1–2 % level, e.g., the Karlsruhe 4π BaF_2 detector.[11]

Instead of absolute activation measurements based on the induced ^{7}Be activity, it is often convenient to perform activations relative to gold with the investigated sample sandwiched between gold foils. As all previous relative activations were performed with flat samples, the associated systematic uncertainties have to be discussed in the light of the present study, where the use of a spherical sample was found to be a crucial point. In this context two problems need to be discussed to ensure that the relative measurements remain valid.

(i) The use of flat samples gives a larger weight to the neutron spectra emitted at larger angles, corresponding to a deformation of the integral spectrum of Fig. 3. However, even this modified spectrum is well fitted by a Maxwell distribution for $kT = 25.0$ keV, so that the average neutron energy in these relative activations is still correct.

(ii) The effective gold cross section for the quasistellar neutron spectrum obtained from the ^{7}Li(p,n)^{7}Be reaction at $E_p = 1912$ keV is 586±8 mb. The investigated cross section must then be corrected for the fact that the experimental spectrum is truncated at 110 keV. For gold this requires multiplication with the factor $K_{\text{spec}} = \langle \sigma_1 \rangle / \langle \sigma_3 \rangle = 0.980$ (as in Eq. 6). This factor is also influenced by the energy dependence of the cross section, which can be parametrized as E_n^{-x}. The above correction holds exactly for gold ($x = 0.6$), but would only change to 0.984 for $x = 0.5$. Therefore, this effect can be neglected in most cases. Where differential data are not available for an estimate of x, activation via the ^{3}H(p,n)^{3}He reaction might be used to obtain a second stellar cross section at $kT = 52$ keV.[15]

On the basis of the new gold cross section, all previous cross sections reported from the Karlsruhe Van de Graaff have been renormalized as gold was always used as a standard.[18] From this list, Table V presents those data which had to be changed by more than 50% of the respective uncertainties. In column 1 the data appear as they were quoted in the compilation of Bao and Käppeler.[9] The only new result is the krypton cross section of Käppeler *et al.*,[15] which is marked with a footnote a in the table. The renormalization procedure always started from the original literature. Results from

TABLE V. Capture cross sections from the Karlsruhe Van de Graaff, renormalized according to the new gold cross section. Only those cases were considered where the values quoted by Bao and Käppeler (Ref. 9) had to be changed by more than 50% of the respective uncertainties. Partial cross sections to isomeric states are marked (p).

Isotope	Bao and Käppeler (mb)	Renormalized value (mb)	New recommended cross section (mb)
^{70}Ge	86.7±5.0	90±4	90±4
^{80}Kr	242±14	251±9	251±9
^{83}Kr	237±15	245±13	245±13
^{84}Kr	19.0±2.4 (p)	18.7±2.3 (p)	
	16.7±1.2[a] (p)	17.3±1.1	17.6±1.1 (p)
^{86}Sr	70±4	73±4	73±4
^{93}Nb	252±13	261±9	273±15
^{103}Rh	772±39	800±27	850±50
^{114}Cd	114±8 (p)	120±8 (p)	120±8 (p)
^{143}Nd	242±10	253±10	253±10
^{152}Sm	378±23	396±22	396±22
^{156}Dy	1445±145	1576±150	1576±150
^{163}Dy	1153±44	1140±32	1140±38
^{170}Yb	738±29	730±22	
	706±28	748±26	739±22
^{175}Lu	1179±44	1166±37	
	1166±40	1236±34	1203±40
^{175}Lu	744±44 (p)	788±46 (p)	788±46 (p)
^{176}Lu	1514±56	1497±40	
	1583±78	1639±85	1537±60
^{181}Ta	726±36	752±30	
	884±46	916±50	742±30
^{184}W	236±9	244±9	230±10
^{197}Au	562±20		582±9

[a]Reference 15.

activation measurements are now based on the new Maxwellian average for gold, which implies that the correction for the truncated experimental neutron spectrum assumes the same cross section shape as for gold (E_n^{-x}, $x=0.6$); possible differences in the exponent x were neglected (see Sec. IV). However, a 1.8% uncertainty was considered for extrapolation from $kT=25$ to 30 keV, which accounts for the difference between cross section slopes according to $x=0.5$ and 0.6. In general, the renormalized cross sections are slightly smaller and do show smaller uncertainties (column 2). The new recommended cross sections (column 3) were then obtained by combination of the renormalized data with other results from literature.[9]

VI. SUMMARY

The quasistellar neutron spectrum that can be obtained with the ^{7}Li(p,n)^{7}Be reaction was reinvestigated with improved accuracy. In particular, it was shown that the spectrum follows the Maxwellian shape down to 1 keV neutron energy, and that it is not very sensitive to proton energy. The corresponding thermal energy is $kT=25.0\pm0.5$ keV.

The average neutron capture cross section of ^{197}Au was measured in this spectrum to 586 mb ±1.4% via activation. To achieve this precision, all relevant parameters were investigated experimentally, and the final activations were carried out under widely different conditions.

The measured cross section was transformed to the true stellar value for $kT=30$ keV by means of the differential cross sections of Macklin (1982): $\langle\sigma v\rangle/v_T=582\pm9$ mb. In turn, this result was used for renormalization of the differential gold cross section of Macklin[2] as well as of previous gold based measurements from the Karlsruhe Van de Graaff.

ACKNOWLEDGMENT

We thank H. Roller and G. Rupp for their patient technical assistance during this somewhat iterative experiment. We are also indebted to R. L. Macklin for helpful comments and to H. Beer for pointing out an inconsistency in the renormalization of the previous gold based results.

*On leave from Institute for Nuclear Studies, Swierk, Poland.
[1]B. J. Allen, J. H. Gibbons, and R. L. Macklin, Adv. Nucl. Phys. **4**, 205 (1971).
[2]R. L. Macklin, private communication.
[3]J. B. Czirr and M. L. Stelts, Nucl. Sci. Eng. **52**, 299 (1973).
[4]R. Gwin, E. G. Silver, R. W. Ingle, and H. Weaver, Nucl. Sci. Eng. **59**, 79 (1976).
[5]V. N. Kononov, B. D. Yurlov, G. E. Manturov, E. D. Poletaev, and V. M. Tomokhov, Yad. Fiz. **26**, 947 (1977).
[6]S. Zhu, S. Jiang, Y. Chen, and D. Luo, Chin. J. Nucl. Phys. **6**, 23 (1984).
[7]N. Yamamuro, M. Igashira, T. Sekiya, and H. Shirayanagi, J. Nucl. Sci. Technol. **20**, 797 (1983).
[8]R. L. Macklin, J. Halperin, and R. R. Winters, Phys. Rev. C **11**, 1270 (1975).
[9]Z. Y. Bao and F. Käppeler, At. Data Nucl. Data Tables **36**, 411 (1987).
[10]W. P. Poenitz, J. Nucl. Energy **20**, 825 (1966).
[11]F. Käppeler, G. Schatz, and K. Wisshak, Kernforschungszentrum Karlsruhe Report KfK-3472, 1983.
[12]K. Wisshak, F. Käppeler, and H. Müller, Nucl. Instrum. Methods **A251**, 101 (1986).
[13]H. Beer and F. Käppeler, Phys. Rev. C **21**, 534 (1980).
[14]H. Beer, private communication.
[15]F. Käppeler, A. A. Naqvi, and M. Al-Ohali, Phys. Rev. C **35**, 936 (1987).
[16]*Table of Isotopes,* edited by C. M. Lederer and V. S. Shirley (Wiley, New York, 1978).
[17]R. T. Skelton and R. W. Kavanagh, Nucl. Phys. **A414**, 141 (1984).
[18]W. Ratynski and F. Käppeler, Kernforschungszentrum Karlsruhe internal report, 1987.

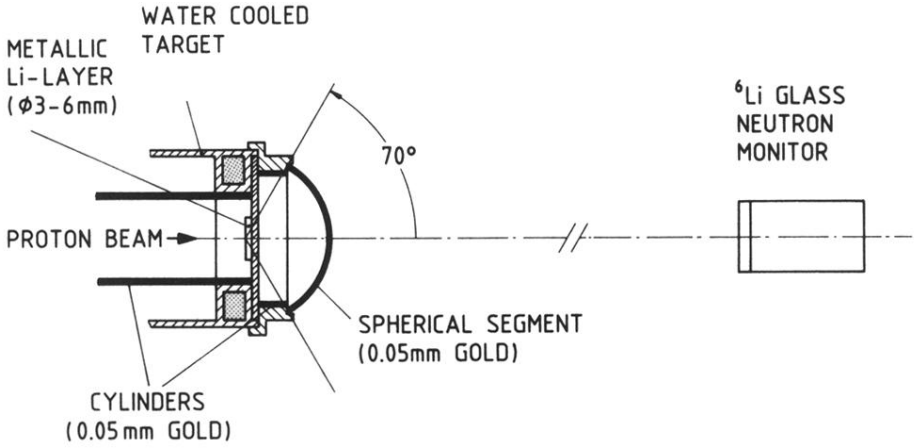

FIG. 5. Experimental setup during the activations. In addition to the spherical gold sample, two gold cylinders were used to detect the effect of scattered neutrons. The sample upstream of the neutron target acts also as a catcher for ^{7}Be sputtered from the target.